

Ab initio calculation of (2+1) resonance enhanced multiphoton ionization spectra and lifetimes of the $(D,3)^2\Sigma^-$ states of OH and OD

Mark P. J. van der Loo and Gerrit C. Groenenboom^{a)}

Institute of Theoretical Chemistry, University of Nijmegen, Toernooiveld 1, 6525ED, Nijmegen, The Netherlands

(Received 2 May 2005; accepted 17 June 2005; published online 22 August 2005)

High-level *ab initio* potential-energy curves and transition dipole moments for the OH $X^2\Pi$, $2^2\Pi$, $1^2\Sigma^-$, $D^2\Sigma^-$, $3^2\Sigma^-$, $A^2\Sigma^+$, $B^2\Sigma^+$, $1^2\Delta$, $1^4\Sigma^-$, and $1^4\Pi$ states are computed. The results are used to estimate the (2+1) resonance enhanced multiphoton ionization spectrum for the

$(D,3)^2\Sigma^-(v') \leftarrow X^2\Pi(v'')$ transitions, which are compared with experiments by Greenslade *et al.* [see M. E. Greenslade, M. I. Lester, D. C. Radenovic, J. A. van Roij, and D. H. Parker, *J. Chem. Phys.* **123**, 074309 (2005), preceding paper]. We use the discrete variable representation-absorbing boundary condition method to incorporate the effect of the dissociative intermediate $1^2\Sigma^-$ state. We obtain qualitative agreement with experiment for the line strengths. Radiative and predissociative decay rates of the Rydberg $(D,3)^2\Sigma^-$ states of OH and OD were computed, including spin-orbit coupling effects and the effect of spin-electronic and gyroscopic coupling. We show that the lifetime of the Rydberg $^2\Sigma^-$ states for rotationally cold molecules is limited mainly by predissociation caused by spin-orbit coupling. © 2005 American Institute of Physics. [DOI: 10.1063/1.1997133]

I. INTRODUCTION

The first observation of the Rydberg $D^2\Sigma^-$ state of OH was reported by Douglas¹ in 1974, while the first theoretical potential-energy curves of the $D^2\Sigma^-$ and $3^2\Sigma^-$ states were reported one year earlier by Easson and Price.² The Rydberg $D^2\Sigma^-$ and $3^2\Sigma^-$ states have been studied experimentally³⁻⁵ and theoretically⁶⁻⁸ ever since by various authors. In 1983, van Dishoeck *et al.*⁶ reported the first extensive theoretical description of the $D^2\Sigma^-$ state. The electronic assignments $D^2\Sigma^-(1\pi^23p\sigma)$ and $3^2\Sigma^-(1\pi^24s\sigma)$ are discussed in Ref. 7. The need for a good description of the ~ 10 eV energy region of OH/D for astrophysical applications has long since been recognized⁹⁻¹¹ and is still relevant today.¹² Recently a sensitive OH/D detection scheme based on the one-photon $D^2\Sigma^- \leftarrow X^2\Pi$ transition was proposed.⁵

The present work was directly motivated by the recent two-photon resonant, resonance enhanced multiphoton ionization [(2+1) REMPI] experiments performed on rotationally cold, state-selected OH[$X^2\Pi(v, J=|M_J|=|\Omega|=3/2)$] radicals by Greenslade *et al.*, which are described in the accompanying paper.¹³ We refer to this paper as Paper I. The purpose of our work is to explain why certain transitions were observed, and others not, and to estimate the absolute sensitivity of the experimental method. The lifetimes of the Rydberg $^2\Sigma^-$ states are still only estimated very crudely in various papers.^{3,5} Here, we elucidate the (non)radiative decay mechanisms of the Rydberg $^2\Sigma^-$ states to accurately estimate the lifetimes of these states for OH and OD.

In Sec. II A we describe the calculation of a new set of potential-energy curves and electronic transition dipole mo-

ments, computed at the multireference configuration interaction level, for all electronic states up to and including the $3^2\Sigma^-$ state (see Figs. 1 and 2). In order to describe the (2+1) REMPI spectrum, we derive in Sec. II B a rate model that includes the two-photon excitation, the detection step, and the competition of the detection step with the decay of the excited states. We use second-order perturbation theory (Sec. II B 1) to estimate the two-photon absorption cross sections and to compare the relative intensities for different vibronic transitions.

Since the experiment is performed on state-selected, aligned molecules, we also derive the equations that relate the two-photon absorption strength to the direction and polarization of the laser beam with respect to the (space-fixed) quantization axis of the total molecular angular momentum.

Calculating the two-photon absorption cross sections for $(D,3)^2\Sigma^- \leftarrow X^2\Pi$ transitions involves an integral over the nuclear states of the dissociative $1^2\Sigma^-$ state. In Sec. II B 2 we show how the discrete variable representation-absorbing boundary condition (DVR-ABC) method of Seideman and Miller^{14,15} and Seideman¹⁶ can be applied to treat this problem numerically. In Sec. II B 3 we discuss the calculation of the decay rates of rovibrational Rydberg $(D,3)^2\Sigma^-$ states associated with several homogeneous and heterogeneous predissociation processes.

II. THEORY

We describe the wave function in terms of eigenfunctions of the nonrelativistic molecular Hamiltonian \hat{H} :

^{a)}Author to whom correspondence should be addressed. Electronic mail: gerritg@theochem.ru.nl

$$\hat{H} = \hat{T}_{\text{nuc}} + \hat{H}_{\text{elec}}, \quad (1)$$

where \hat{H}_{elec} represents the nonrelativistic electronic Hamiltonian in the clamped-nuclei approximation and \hat{T}_{nuc} is the nuclear kinetic-energy operator, which can be written as the sum of a radial (\hat{T}_r) and a rotational part \hat{H}_{rot} :

$$\hat{T}_{\text{nuc}} = \hat{T}_r + \hat{H}_{\text{rot}} = \frac{-\hbar^2}{2\mu r} \frac{\partial^2}{\partial r^2} + \frac{\hat{\mathbf{R}}^2}{2\mu r^2}, \quad (2)$$

where r is the internuclear distance, μ is the reduced mass of the system, and $\hat{\mathbf{R}} \equiv \hat{\mathbf{J}} - \hat{\mathbf{S}} - \hat{\mathbf{L}}$ describes the nuclear angular momentum operator acting on the polar angle β and the azimuthal angle α of the diatomic axis in the space-fixed frame. The operators $\hat{\mathbf{J}}$, $\hat{\mathbf{S}}$, and $\hat{\mathbf{L}}$ represent the total angular momentum apart from the nuclear spin, the electronic spin, and the electronic orbital angular momentum, respectively. At low rotational levels, the Π states of OH/D approach the Hund's case (a) limit, while multiplets of Σ symmetry are formally pure Hund's case (b) states.¹⁷ Since in this work we describe the OH/D molecule at only the lowest rotational levels, we use the pure case (a) description for Π states and the pure case (b) description for Σ states. Hund's case (a) and (b) wave functions of parity p are given by

$$|v; JM_J \Omega(L) \Lambda S \Sigma p\rangle = \frac{[1 + (-1)^p \hat{i}] \chi_v^a(r)}{\sqrt{(2 + \delta_{\Lambda 0} \delta_{\Sigma 0})}} |JM_J \Omega(L) \Lambda S \Sigma\rangle, \quad (3)$$

$$|v; JM_J N(L) \Lambda S p\rangle = \frac{[1 + (-1)^p \hat{i}] \chi_v^b(r)}{\sqrt{(2 + \delta_{\Lambda 0})}} |JM_J N(L) \Lambda S\rangle, \quad (4)$$

where J , M_J , Ω , N , Λ , and S are the usual Hund's case (a) and (b) quantum numbers.¹⁸ The nuclear wave functions ($\chi_v^{a/b}$) are labeled with the vibrational quantum number v , which is replaced by the energy E for continuum states. The superscripts (a) and (b) represent all case (a) and case (b) quantum numbers. States with parity $(-1)^{J-1/2}$ and $(-1)^{J+1/2}$ are labeled by e and f, respectively. The electronic orbital angular momentum L is not a good quantum number. However, we use (L) to indicate its value in the atomic limit. We will also use the labels F_1 and F_2 to indicate Hund's case (b) states with $N=J+\frac{1}{2}$ and $N=J-\frac{1}{2}$, respectively. We use the phase conventions defined in the Appendix of Ref. 19 to obtain the action of the inversion operator \hat{i} :

$$\hat{i}|JM_J \Omega(L) \Lambda S \Sigma\rangle = (-1)^{J+L-S} |JM_J - \Omega(L) - \Lambda S - \Sigma\rangle, \quad (5)$$

$$\hat{i}|JM_J N(L) \Lambda S\rangle = (-1)^{N+L} |JM_J N(L) - \Lambda S\rangle. \quad (6)$$

The rotronic Hund's case (a) and (b) basis functions are given by

$$|JM_J \Omega(L) \Lambda S \Sigma\rangle = \sqrt{[J]/4\pi} D_{M_J \Omega}^{(J)*}(\alpha, \beta, 0) |(L) \Lambda S \Sigma\rangle, \quad (7)$$

TABLE I. Details of the *ab initio* calculations.

State ^a	Basis ^b	Space ^c	SA-CASSCF ^d
$X^2\Pi$	aV6Z	$5\sigma 2\pi$	
$A^2\Sigma^+, 1^2\Sigma^-$	aV6Z	$5\sigma 2\pi$	
$1^4\Sigma^-$	aV6Z	$6\sigma 1\pi$	
$1^4\Pi$	aV6Z	$6\sigma 1\pi$	
$1^2\Delta$	aV6Z	$5\sigma 2\pi$	$1^2\Sigma^-(1/4)$
$D^2\Sigma^-$	daV5Z	$6\sigma 2\pi$	$1^2\Sigma^-, 1^2\Delta(1/2:1/4)$
$3^2\Sigma^-$	daV5Z	$6\sigma 2\pi$	$1^2\Delta, (1, D)^2\Sigma^-$
$2^2\Pi$	daV5Z	$5\sigma 2\pi$	$X^2\Pi_{x,y}(1/4)$
$B^2\Sigma^+$	daVTZ	$5\sigma 2\pi$	$A^2\Sigma^+, 1^2\Delta$
$\langle X^2\Pi \hat{d} 1^2\Sigma^- \rangle$	aV6Z	$5\sigma 2\pi$	
$\langle X^2\Pi \hat{d} A^2\Sigma^+ \rangle$	aV6Z	$5\sigma 2\pi$	
$\langle 1^2\Sigma^- \hat{d} D^2\Sigma^- \rangle$	daV5Z	$6\sigma 1\pi$	$1^2\Delta$
$\langle 1^2\Sigma^- \hat{d} 3^2\Sigma^- \rangle$	daV5Z	$6\sigma 1\pi$	$1^2\Delta, D^2\Sigma^-$
$\langle X^2\Pi \hat{d} D^2\Sigma^- \rangle$	daV5Z	$6\sigma 1\pi$	$1^2\Sigma^-, 1^2\Delta$
$\langle X^2\Pi \hat{d} 3^2\Sigma^- \rangle$	daV5Z	$6\sigma 1\pi$	$1^2\Delta, (1, D)^2\Sigma^-$
$\langle 3^2\Sigma^- \hat{d} D^2\Sigma^- \rangle$	daV5Z	$6\sigma 2\pi$	$1^2\Sigma^-, 1^2\Delta$
$\langle (D, 3)^2\Sigma^- \hat{H}_{\text{sol}} 2^2\Pi \rangle$	daVTZ	$5\sigma 1\pi$	$X^2\Pi_{x,y}, 1^2\Sigma^-, 1^2\Delta$
$\langle (D, 3)^2\Sigma^- \hat{H}_{\text{sol}} B^2\Sigma^+ \rangle$	daVTZ	$5\sigma 1\pi$	$A^2\Sigma^+, 1^2\Sigma^-, 1^2\Delta$
$\langle (D, 3)^2\Sigma^- \hat{H}_{\text{sol}} 1^4\Pi \rangle$	daVTZ	$5\sigma 1\pi$	$1^2\Sigma^-, 1^2\Delta$

^aThe electronic state or the matrix element. We used Davidson's correction (Ref. 51) for the $(D, 3)^2\Sigma^-, 2^2\Pi$, and $B^2\Sigma^+$ states. The L_{\pm} matrix elements are obtained from the same calculation as the spin-orbit matrix elements.

^bThe one-electron basis sets are of the (doubly) augmented correlation-consistent polarized valence triple-zeta, 5-zeta, or 6-zeta [(d)av(T,5,6)Z] type (Ref. 52). For the spin-orbit and L_{\pm} matrix elements uncontracted basis sets are used.

^cThe active space used in the SA-CASSCF calculation: $n\sigma$ means that the $2\sigma-n\sigma$ orbitals are included (the 1σ orbital is kept doubly occupied in all calculations) and $n\pi$ means that the $1\pi_{x,y}-n\pi_{x,y}$ orbitals were used.

^dStates also included in the SA-CASSCF calculation. All states have equal weights, unless otherwise indicated. The states in the first column always have weight equal to 1.

$$|JM_J N(L) \Lambda S\rangle = \sum_{M_N M_S} \sqrt{[N]/4\pi} D_{M_N \Lambda}^{(N)*}(\alpha, \beta, 0) |(L) \Lambda\rangle |SM_S\rangle \times \langle NM_N SM_S | JM_J \rangle, \quad (8)$$

where $\sqrt{[N]/4\pi} D_{M_N \Lambda}^{(N)*}(\alpha, \beta, 0)$ represents a two-angle normalized Wigner D -matrix and $[X] \equiv 2X+1$.

A. Electronic structure calculations

Ab initio potential-energy curves for the OH $X^2\Pi$, $2^2\Pi$, $1^2\Sigma^-, D^2\Sigma^-, 3^2\Sigma^-, A^2\Sigma^+, B^2\Sigma^+, 1^4\Sigma^-, 1^4\Pi$, and $1^2\Delta$ states are computed with the MOLPRO²⁰ program package at the internally contracted multireference configuration interaction (MRCI) with single and double excitations^{21,22} level. The molecular orbitals are obtained from state-averaged complete active space self-consistent field (SA-CASSCF) calculations.^{23,24} We also computed the the Breit-Pauli²⁵ spin-orbit coupling and \hat{L}_{\pm} matrix elements and the r -dependent electronic transition dipole moments at the SA-CASSCF+MRCI level. Details of the *ab initio* calculations are given in Table I.

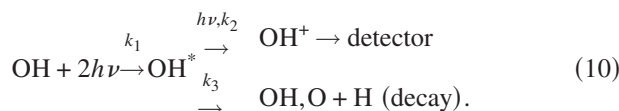
All *ab initio* points are interpolated using cubic splines. To improve our ability to predict the position of unobserved vibrational levels, we also apply a linear scaling of the form

$$V_{sc}(r) = c_3 V(r'), \quad r' = c_2 + c_3 r \quad (9)$$

to the potentials $V(r)$ of the $D^2\Sigma^-$ and $3^2\Sigma^-$ states. The scaling parameters c_1 , c_2 , and c_3 are obtained by a nonlinear fitting procedure that minimizes the relative error in calculated vibrational spacings and rotational B_v constants. The $D^2\Sigma^-$ and $3^2\Sigma^-$ state curves are shifted to match the experimentally observed OH[$(D,3)^2\Sigma^-(v=0) \leftarrow X^2\Pi(v=0)$] transition frequencies. The dissociative curves are shifted to match the atomic energies²⁶ at $10a_0$, and the $B^2\Sigma^+$ potential-energy curve was shifted to match the experimental OH[$B^2\Sigma^+(v'=0) \leftarrow X^2\Pi(v''=7)$] transitions as reported by Copeland *et al.*²⁷

B. (2+1) REMPI

The use of rate models to describe the production and detection of ions in resonant multiphoton ionization processes is well established.^{28–32} The (2+1) REMPI process as described in Paper I may be summarized schematically as follows:



The state-selected OH molecule is first two-photon excited at rate k_1 , after which it is either ionized (rate k_2) with a third photon and detected as OH^+ or it decays (rate k_3) and the molecule is lost for detection. The rate coefficients in s^{-1} are given by

$$k_1 = g^{(2)} \sigma^{(2)}(\omega) [I/\hbar\omega]^2, \quad (11)$$

$$k_2 = \sigma_{\text{ion}}(\omega) I/\hbar\omega, \quad (12)$$

$$k_3 = \tau_{\text{OH}^*}^{-1}, \quad (13)$$

where $\sigma^{(2)}$ is the generalized two-photon absorption cross section in $\text{cm}^4 \text{s}$, I is the laser intensity in W/cm^2 , ω is the laser angular frequency in s^{-1} , σ_{ion} is the excited-state ionization cross section in cm^2 , and τ_{OH^*} is the lifetime of the excited state in seconds. The coherence factor $g^{(2)}$ for two-photon absorption is 1 if the molecule is excited with coherent light and 2 for chaotic light.^{33,34} We employ two extreme cases of this model to estimate the two-photon absorption strength. In the first extreme detection is very efficient, so we have $k_2 \gg k_3$ and the number of detected OH^+ molecules $[\text{OH}^+] \propto k_1$. In the other extreme, decay is faster than detection and we have $[\text{OH}^+] \propto k_1 k_3^{-1}$. We assume a constant measurement time for all observations and an abundance of OH molecules in the molecular beam such that no saturation occurs. In the case of fast ionization, we obtain

$$[\text{OH}^+] \propto g^{(2)} (I/\hbar\omega)^2 \hat{\sigma}^{(2)}, \quad (14)$$

and in the case of fast decay

$$[\text{OH}^+] \propto g^{(2)} (I/\hbar\omega)^2 \tau_{\text{OH}^*}^{-1} \hat{\sigma}^{(2)}, \quad (15)$$

where $\hat{\sigma}^{(2)}$ is the integrated line cross section for two-photon absorption:³⁵

$$\hat{\sigma}^{(2)} = \int d\omega \sigma^{(2)}(\omega). \quad (16)$$

1. Two-photon absorption

The generalized two-photon absorption cross section $\sigma_{fi}^{(2)}$ in rationalized mks (Ref. 36) units is given by^{33,34,37,38}

$$\sigma_{J'M_J f; J''M_J i}^{(2)}(\omega) = \frac{(2\pi)^3 \alpha^2 \omega^2}{e^4} S_{J'M_J f; J''M_J i}^{(2)} \times \delta(\omega_i - \omega_f + 2\omega), \quad (17)$$

where ω is the excitation angular frequency, α is the fine-structure constant, and e is the elementary charge. Labels i and f indicate initial and final quantum numbers v, Ω, L, Λ, S , and Σ for a Hund's case (a) function and v, N, L, Λ , and S for a Hund's case (b) function. Here, we suppress the parity label p . The two-photon line strength $S^{(2)}$ is given by

$$S_{J'M_J f; J''M_J i}^{(2)} = \hbar^2 \lim_{\varepsilon \downarrow 0} \left| \sum_E \frac{\langle \psi_f^{J'M_J} | \boldsymbol{\varepsilon} \cdot \hat{\boldsymbol{\mu}} | \psi_E \rangle \langle \psi_E | \boldsymbol{\varepsilon} \cdot \hat{\boldsymbol{\mu}} | \psi_i^{J''M_J} \rangle}{E_{\text{ph}} + E_i - E + i\varepsilon/2} \right|^2, \quad (18)$$

where $E_{\text{ph}} = \hbar\omega$ is the one-photon energy. The complete set of intermediate states ψ_E includes both continuum (dissociative) states and discrete (bound) states. The symbol \sum_E signifies the integration over the continuum intermediate states and a summation over the discrete intermediate states. We take the propagation direction of the molecular beam as the space-fixed z axis. The laser polarization $\boldsymbol{\varepsilon}$ and the electronic dipole operator $\hat{\boldsymbol{\mu}}$ are defined in this frame. The spherical components of $\boldsymbol{\varepsilon}$ are given by

$$\varepsilon_q = \sum_p D_{qp}^{(1)*}(\phi, \theta, \chi) \tilde{\boldsymbol{\varepsilon}}_p, \quad (19)$$

where (ϕ, θ, χ) are the zyz -Euler angles of the laser frame with respect to the space-fixed frame and $\tilde{\boldsymbol{\varepsilon}}$ is the polarization vector in the laser frame.

Applying the Wigner-Eckart theorem¹⁸ and recoupling the angular momenta, we rewrite Eq. (18) as follows:

$$\begin{aligned} & \sum_E \frac{\langle \psi_f^{J'M_J} | \boldsymbol{\varepsilon} \cdot \hat{\boldsymbol{\mu}} | \psi_E \rangle \langle \psi_E | \boldsymbol{\varepsilon} \cdot \hat{\boldsymbol{\mu}} | \psi_i^{J''M_J} \rangle}{E_{\text{ph}} + E_i - E + i\varepsilon/2} \\ &= \sum_{Jkq} (-1)^{J''+M_J} \sqrt{[k]} \mathcal{E}_q^{(k)} \begin{Bmatrix} J'' & 1 & J \\ 1 & J' & k \end{Bmatrix} \\ & \times \begin{pmatrix} J' & k & J'' \\ -M_{J'} & -q & M_{J''} \end{pmatrix} \sum_E \frac{\langle \psi_f^{J'} \| \hat{\boldsymbol{\mu}}^{(1)} \| \psi_E' \rangle \langle \psi_E' \| \hat{\boldsymbol{\mu}}^{(1)} \| \psi_i^{J''} \rangle}{E_{\text{ph}} + E_i - E + i\varepsilon/2}, \end{aligned} \quad (20)$$

where $\mathcal{E}^{(k)} = [\boldsymbol{\varepsilon} \otimes \boldsymbol{\varepsilon}]^{(k)}$ is the two-photon polarization tensor.¹⁸ Since the $X^2\Pi$ ground state approaches the Hund's case (a) limit, we need both the reduced matrix elements for a Hund's case (b) \leftarrow (a) transition as well as the reduced matrix element for a Hund's case (b) \leftarrow (b) transition. The Hund's case (b) \leftarrow (a) reduced matrix element reads

$$\begin{aligned} \langle \psi_b' | \hat{\mu}^{(1)} | \psi_a' \rangle &= \langle \chi_v^b | \hat{d}_{\Lambda-\Lambda'}^{(1)} | \chi_{v'}^{a'} \rangle \\ &\times \delta_{SS'} (-1)^{2J} \sqrt{[N][J][J']} \sum_{\Omega'} \begin{pmatrix} J & 1 & J' \\ -\Omega & t & \Omega' \end{pmatrix} \\ &\times \begin{pmatrix} J & S & N \\ -\Omega & \Sigma' & \Lambda \end{pmatrix}, \end{aligned} \quad (21)$$

while the Hund's case (b) ← (b) reduced matrix element is given by

$$\begin{aligned} \langle \psi_b' | \hat{\mu}^{(1)} | \psi_a' \rangle &= \langle \chi_v^b | \hat{d}_{\Lambda-\Lambda'}^{(1)}(r) | \chi_{v'}^{a'} \rangle \\ &\times \delta_{SS'} (-1)^{J'+S-\Lambda+1} \sqrt{[N][N'][J][J']} \\ &\times \begin{Bmatrix} J & N & S \\ N' & J' & 1 \end{Bmatrix} \begin{pmatrix} N & 1 & N' \\ -\Lambda & \Lambda - \Lambda' & \Lambda' \end{pmatrix}. \end{aligned} \quad (22)$$

The body-fixed dipole operator $\hat{\mathbf{d}}$ is implicitly defined by $\hat{\mu}_p^{(1)} = \sum_q D_{pq}^{(1)*}(\alpha, \beta, 0) \hat{d}_q^{(1)}$.

Since the experiments described in Paper I are performed on rotationally cold molecules, we neglect rotational effects on the radial wave functions in the calculation of the two-photon transition strengths. The dominant terms in the coherent sum are the states which are (nearly) resonant with the one-photon energy, so we estimate the relative two-photon line strength by taking into account the electronic states computed in this work. The optically allowed intermediate states are the $X^2\Pi$, $2^2\Pi$, $1^2\Sigma^-$, $D^2\Sigma^-$, and $3^2\Sigma^-$ states. We neglect the contributions of vibrational levels of the initial and final electronic states, as well as contributions of the $2^2\Pi$ state which has a small Frank-Condon overlap with the final states. The remaining two intermediate states [$(1^2\Sigma^-, D^2\Sigma^-)$ or $(1^2\Sigma^-, 3^2\Sigma^-)$] are of $2^2\Sigma^-$ symmetry, so the cross section factorizes in a radial factor $\sigma_{fi}^{(2)}$ and a dimensionless angular factor S :

$$\sigma_{J'M_{Jf}; J''M_{Ji}}^{(2)}(\omega) = \sigma_{fi}^{(2)}(\omega) S_{J''M_{J''}\Omega''\Lambda''}^{J'M_{J'}N'\Lambda'} \delta(\omega_i - \omega_f + 2\omega), \quad (23)$$

where $\sigma_{fi}^{(2)}(\omega)$ is found from Eqs. (17)–(23):

$$\begin{aligned} \sigma_{fi}^{(2)}(\omega) &= \frac{\hbar^2 (2\pi)^2 \alpha^2 \omega^2}{e^4} \\ &\times \left| \sum_{Em} \frac{\langle \chi_{v'}^f | \hat{d}_{\Lambda'-\Lambda} | \chi_E^m \rangle \langle \chi_E^m | \hat{d}_{\Lambda-\Lambda'} | \chi_{v'}^i \rangle}{E_{\text{ph}} + E_{iv'} - E + i\varepsilon/2} \right|^2, \end{aligned} \quad (24)$$

where we added the vibrational quantum numbers for clarity. The summation is over the vibrational levels of the $3^2\Sigma^-$ state for transition to the $D^2\Sigma^-$ state and vice versa, and the integration is over the $1^2\Sigma^-$ nuclear continuum. The angular factor for a Hund's case (b) ← (b) ← (a) two-photon transition can be written as

$$\begin{aligned} S_{J''M_{J''}\Omega''\Lambda''}^{J'M_{J'}N'\Lambda'} &= [N'][J'][J''] \left| \sum_{JN} (-1)^{\varphi} [N][J] \right. \\ &\times \left(\sum_{kq} [k]^{1/2} \mathcal{E}_{pq}^{(k)} \begin{pmatrix} J' & k & J'' \\ -M_{J'} & -q & M_{J''} \end{pmatrix} \right. \\ &\times \left. \begin{Bmatrix} J'' & 1 & J \\ 1 & J' & k \end{Bmatrix} \right) \left. \begin{Bmatrix} J' & N' & S \\ N & J & 1 \end{Bmatrix} \right. \\ &\times \left. \begin{pmatrix} N' & 1 & N \\ -\Lambda' & \Lambda' - \Lambda & \Lambda \end{pmatrix} \sum_{\Omega'} \begin{pmatrix} J & 1 & J'' \\ \Omega & t & \Omega'' \end{pmatrix} \right. \\ &\times \left. \begin{pmatrix} J & S & N \\ -\Omega & \Sigma'' & \Lambda \end{pmatrix} \right|^2, \end{aligned} \quad (25)$$

where $\varphi = J'' + M_{J''} - J + S - \Lambda' + 1$.

2. Numerical treatment

The bound-state nuclear wave functions are represented on a grid using the sinc-function discrete variable representation (sinc-DVR).^{39,40} The contributions of the optically active bound intermediate states to the two-photon transitions are computed using the relevant transition dipole moments depicted in Fig. 2. Summing over five vibrational levels of the intermediate Rydberg $2^2\Sigma^-$ states converges the calculations. Evaluating the contribution of the dissociative $1^2\Sigma^-$ intermediate state poses two problems: first, there is an integral over nuclear states and second, the integrand is singular at the one-photon resonance. However, a numerical treatment is possible when the resolvent is rewritten as follows:

$$\begin{aligned} \int dE \frac{|\chi_E^{1^2\Sigma^-}\rangle \langle \chi_E^{1^2\Sigma^-}|}{E^* - E + i\varepsilon/2} &= \lim_{\varepsilon \downarrow 0} [E^* - (T_r + \hat{V}_{1^2\Sigma^-}) + i\varepsilon/2]^{-1} \\ &= \hat{G}(E^*), \end{aligned} \quad (26)$$

where \hat{G} is the Green operator, $E^* = E_{\text{ph}} + E_{iv'}$, and we used (neglecting spin-orbit coupling)

$$[\hat{T}_r + \hat{V}_{1^2\Sigma^-}] |\chi_E^{1^2\Sigma^-}\rangle = E |\chi_E^{1^2\Sigma^-}\rangle. \quad (27)$$

The Green operator can be represented on a grid when we impose absorbing boundary conditions.^{14–16} This is achieved by augmenting the potential $\hat{V}_{1^2\Sigma^-}$ with a negative imaginary potential, which is equivalent to replacing $\varepsilon/2$ by an r -dependent function. Here, we choose the Woods-Saxon potential as a functional form:

$$\lim_{\varepsilon \downarrow 0} \varepsilon/2 \rightarrow \varepsilon(R) = \frac{2\lambda}{1 + \exp[(R_{\text{max}} - R)/\eta]}, \quad (28)$$

where λ and R_{max} are parameters to be adjusted so that the artificial potential does not penetrate the physically relevant region, while η is adjusted so that no significant reflection off the imaginary potential takes place. In this work this is accomplished by setting $\lambda = 0.2E_h$, $R_{\text{max}} = 12a_0$, and $\eta = 0.4a_0$.

3. Decay processes

The Rydberg $2^2\Sigma^-$ states may decay radiatively to the $X^2\Pi$ and $1^2\Sigma^-$ states or through a radiationless process to the $2^2\Pi$, $B^2\Sigma^+$, or $1^4\Pi$ states. The Einstein A coefficient in s^{-1} for a radiative transition is given by³³

$$A_{J'f, J''i}(\omega) = \frac{4\alpha\omega^3}{3c^2e^2[J'']} |\langle \psi_f^{J'} | \hat{\mu}^{(1)} | \psi_i^{J''} \rangle|^2, \quad (29)$$

where the reduced matrix element is given in Eqs. (21) and (22) for Hund's case (b) \rightarrow (a) and Hund's case (b) \rightarrow (b) transitions, respectively, and ω is the angular frequency of the emitted photon. The total radiative lifetime τ_r of a state $\psi_i^{J''}$ is given by

$$\tau_r^{-1} = \sum_f A_{fi} + \int dE A_{fi}(E) \rho(E), \quad (30)$$

where the summation is over all final discrete states and integration is over final continuum states, with $\rho(E)$ the density of final states at energy E . The integral over continuum states is approximated by $\sum_E A_{fi}(E) \Delta E$, where the energy step ΔE is determined by dividing the integration domain for each initial state into 100 integration steps.

Several perturbative processes cause the Rydberg $2^2\Sigma^-$ states to predissociate. Here, we distinguish between heterogeneous predissociation, caused by the gyroscopic coupling from the $\hat{\mathbf{J}} \cdot \hat{\mathbf{L}}$ operator, and homogeneous predissociation, caused by spin-electronic ($\hat{\mathbf{L}} \cdot \hat{\mathbf{S}}$) and spin-orbit coupling (\hat{H}_{so}).

The predissociation lifetime τ_{so} associated with spin-orbit coupling is given by

$$\tau_{so}^{-1} = \frac{2\pi}{\hbar} \sum_f |\langle \psi_f^{M_J} | \hat{H}_{so} | \psi_i^{M_J} \rangle|^2, \quad (31)$$

where the summation runs over all permitted rotronic $B^2\Sigma^+$, $2^2\Pi$, and $1^4\Pi$ states. The calculation of the spin-orbit matrix elements $\langle f | \hat{H}_{so} | i \rangle$ is described in Sec. II A. These matrix elements are computed near the crossing of the two adiabatic Born-Oppenheimer potentials and are assumed constant. The spin-orbit coupling couples the Rydberg states with both the $1^4\Pi_{1/2}(\Lambda=1, \Sigma=-\frac{1}{2})$ and the $1^4\Pi_{1/2}(\Lambda=-1, \Sigma=\frac{3}{2})$ states.

Since the $2^2\Sigma^-$ and the $2^2\Pi$ Rydberg states dissociate adiabatically into different atomic limits, \hat{L}_{\pm} -type couplings between these states are asymptotically zero. However, in the bound region, the \hat{L}_{\pm} operator has nonzero matrix elements so that spin-electronic and gyroscopic coupling contribute to the decay of the Rydberg $2^2\Sigma^-$ states through the $2^2\Pi$ state. Calculation of these matrix elements is described in Sec. II A. We take the matrix elements constant and compute them at a single point near the crossing of two states.

In order to accurately compute the bound state and dissociative wave functions, the adiabatic potential-energy curves are augmented with the relevant centrifugal terms for Hund's case (a) or (b).⁴¹ Bound-state wave functions are computed with the sinc-DVR method^{39,40} and energy-

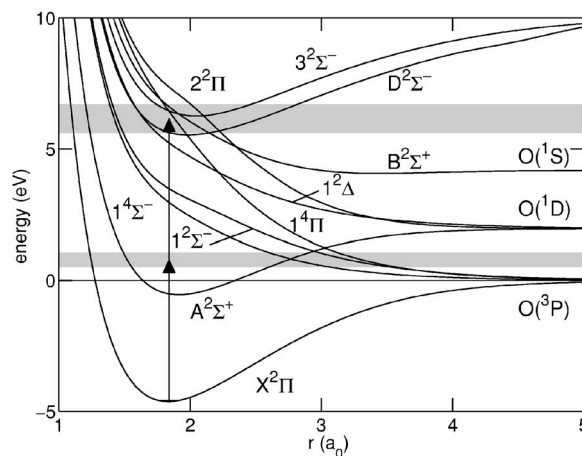


FIG. 1. *Ab initio* potential-energy curves for OH/D (in eV). The gray areas indicate the one-photon and two-photon energy range corresponding to the experiments in Paper I.

normalized dissociative wave functions are computed with the renormalized Numerov method with photodissociation boundary conditions.⁴²

The total lifetime τ is given by $\tau^{-1} = \tau_r^{-1} + \tau_{so}^{-1} + \tau_{se}^{-1} + \tau_{gy}^{-1}$, where τ_{se} and τ_{gy} are the lifetimes associated with spin-electronic and gyroscopic predissociation.

III. RESULTS AND DISCUSSION

A. Electronic structure

Figure 1 depicts the potential-energy curves computed in this work. The quality of the ground-state curve is tested by comparing vibrational levels G_v and rotational constants B_v with recent experimental values by Colin *et al.*⁴³ and Mélen *et al.*⁴⁴ We find errors in G_v which are $<0.1\%$ for $v=0, \dots, 5$ and errors $<0.2\%$ for $v=6, \dots, 10$. The errors in B_v are $<0.06\%$ for $v=0, \dots, 8$ and $<0.2\%$ for $v=9$ and $v=10$. The computed and available experimental values for the Rydberg $(D,3)^2\Sigma^-$ states for OH and OD are shown in Table II. The scaling parameters (c_1, c_2, c_3) [see Eq. (9)] obtained from the fit are $(1.2173 \times 10^{-4}, 0.99199, 1.006)$ for the $D^2\Sigma^-$ state and $(1.6856 \times 10^{-4}, 0.99515, 1.0065)$ for the $3^2\Sigma^-$ state. Although the potentials are changed only very little by these corrections, the improvement in calculated G_v and B_v is substantial. The relative errors for the $D^2\Sigma^-$ state decrease by an order of magnitude to a mean deviation from the experimental G_v to $\sim 0.07\%$. The improvement in G_v and B_v for the $3^2\Sigma^-$ state is large, mainly because of the small number of experimental data available. This implies that extrapolation to $v \geq 2$ should be done with care.

In 1983 van Dishoeck and Dalgarno⁴⁵ stated that the Rydberg $2^2\Sigma^-$ states might predissociate through the $2^2\Pi$ or $B^2\Sigma^+$ states. Apart from these two, the $1^4\Pi$ potential-energy curve also crosses with the $(D,3)^2\Sigma^-$ curves, which yields an extra predissociation process driven by spin-orbit coupling.

Figure 2 shows the r -dependent electronic transition dipole moments calculated in this work. The transition moments were obtained in separate calculations. We took care to have consistent relative signs, since this is essential in the calculation of the two-photon absorption strength [Eq. (24)].

TABLE II. Vibrational spacings G_v and rotational constants B_v for the OH/D Rydberg $2^2\Sigma^-$ states (in cm^{-1}), computed with *ab initio* potentials, scaled *ab initio* potentials, and compared with experimental data (Ref. 13). Tables with more predicted vibrational levels can be downloaded via EPAPS (Ref. 46).

	v	$G(v)$			B_v		
		<i>Ab initio</i>	Scaled	Expt.	<i>Ab initio</i>	Scaled	Expt.
OH							
$D\ 2^2\Sigma^-$	0	0	0	0	15.62	15.37	15.0
	1	2583.05	2570.80	2566	14.86	14.63	14.8
	2	5088.44	5064.70	5067	14.29	14.08	14.2
	3	7519.55	7486.56	7487	13.69	13.49	13.6
$3\ 2^2\Sigma^-$	0	0	0	0	14.83	14.69	14.9
	1	2643.48	2640.00	2640	14.43	14.30	14.1
OD							
$D\ 2^2\Sigma^-$	0	0	0		8.34	8.20	
	1	1902.15	1893.05		8.02	7.90	
	2	3750.35	3732.41		7.78	7.66	
	3	5573.35	5547.26		7.56	7.45	
$3\ 2^2\Sigma^-$	0	0	0		7.89	7.82	
	1	1944.55	1941.80		7.75	7.68	

The most prominent feature in the structure of the transition moments that connect $D\ 2^2\Sigma^-$ and $3\ 2^2\Sigma^-$ states with other states or with each other are the drastic changes around $r = 1.5a_0 - 3a_0$.

Inspection of the coefficients of the most important configurations in the configuration-interaction (CI) wave functions shows that the electronic structure of the $X\ 2^2\Pi$ and $1\ 2^2\Sigma^-$ states do not vary significantly. However, the Rydberg $2^2\Sigma^-$ states show a profound structure change.

Up to $r = 1.5a_0$, the $D\ 2^2\Sigma^-$ state is mainly described as a $|\pi_x\pi_y5\bar{\sigma}|$ configuration. From $1.5a_0$ to $2.0a_0$ the contribution of the $|\pi_x\pi_y5\bar{\sigma}|$ configuration decreases sharply to about 50% of the initial value, while the contribution of the $|\pi_x\pi_y6\bar{\sigma}|$ configuration rises until it is the most important contribution, and the second most important contribution comes from the $|\pi_x\bar{\pi}_y6\bar{\sigma}| + |\bar{\pi}_x\pi_y6\bar{\sigma}|$ linear combination. For interatomic distances larger than $2a_0$ the situation reverses, and around $3a_0$ the $D\ 2^2\Sigma^-$ state is again described almost exclusively by the $|\pi_x\pi_y5\bar{\sigma}|$ configuration. From $4a_0$ to $6a_0$

the coefficient of this configuration drops to zero and the doubly excited $|3\sigma\pi_x\pi_y4\bar{\sigma}5\bar{\sigma}|$ and $|3\sigma\pi_x\pi_y4\bar{\sigma}6\bar{\sigma}|$ configurations become the most important.

In the short range ($1a_0 - 1.5a_0$), the $3\ 2^2\Sigma^-$ state is almost completely described by the $|\pi_x\pi_y6\bar{\sigma}|$ configuration. The importance of this contribution decreases rapidly from $1.5a_0$ to $2.0a_0$, while the $|\pi_x\pi_y5\bar{\sigma}|$ and $|\bar{\pi}_x\pi_y5\bar{\sigma}| + |\pi_x\bar{\pi}_y5\bar{\sigma}|$ configurations rise in importance. From $2a_0$ to $3.5a_0$, the contribution of $|\pi_x\pi_y6\bar{\sigma}|$ increases, while the contribution of the $|\pi_x\pi_y6\bar{\sigma}|$ configuration decreases. At $3.5a_0$ the $3\ 2^2\Sigma^-$ state is described for $\sim 60\%$ by the $|\pi_x\pi_y6\bar{\sigma}|$ configuration and for $\sim 15\%$ by the $|\bar{\pi}_x\pi_y5\bar{\sigma}| + |\pi_x\pi_y5\bar{\sigma}|$ configuration. From $3.5a_0$ to $6a_0$ the $|\pi_x\pi_y5\bar{\sigma}|$ contribution increases at the cost of the $|\pi_x\pi_y6\bar{\sigma}|$ configuration until it is slightly more important (35% against 30%).

All potential-energy curves and transition dipole moments are made available through EPAPS.⁴⁶

B. (2+1) REMPI spectra

Figures 3 and 4 show the simulated and observed two-photon spectra for the $D\ 2^2\Sigma^-(v') \leftarrow X\ 2^2\Pi(v'')$ and $3\ 2^2\Sigma^-(v') \leftarrow X\ 2^2\Pi(v'')$ transitions, respectively. The sticks indicate the relative number of experimental OH⁺ detector counts⁴⁷ for $2^2\Sigma^-(v'J'F_1) \leftarrow X\ 2^2\Pi_{3/2}(v''J''=3/2)\ S_1(1)$ ($J' - J'' = 2$) transitions. The circles and diamonds represent the fast ionization model [Eq. (14)] and the rapid decay case [Eq. (15)], respectively. Both experimental and theoretical intensities were scaled relative to the $(v', v'') = (0, 0)$ transitions. We find an integrated line cross section $\hat{\sigma}^{(2)} = \frac{1}{105} \times 0.27 \times 10^{-35} \text{ cm}^4$ for the $D\ 2^2\Sigma^-(v'=0) \leftarrow X\ 2^2\Pi_{3/2}(v''=0)$ transition and $\hat{\sigma}^{(2)} = \frac{1}{105} \times 0.17 \times 10^{-35} \text{ cm}^4$ for the $3\ 2^2\Sigma^-(v'=0) \leftarrow X\ 2^2\Pi_{3/2}(v''=0)$ transition, where the factor $\frac{1}{105}$ is the angular factor [Eq. (25), Table III] for this transition. However, these numbers are crude estimates due to the limited

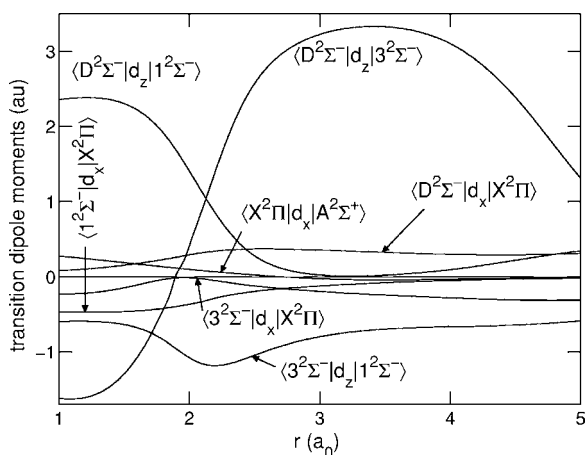


FIG. 2. *Ab initio* Cartesian components of the electronic transition dipole operator for doublet states of OH/D (in a.u.).

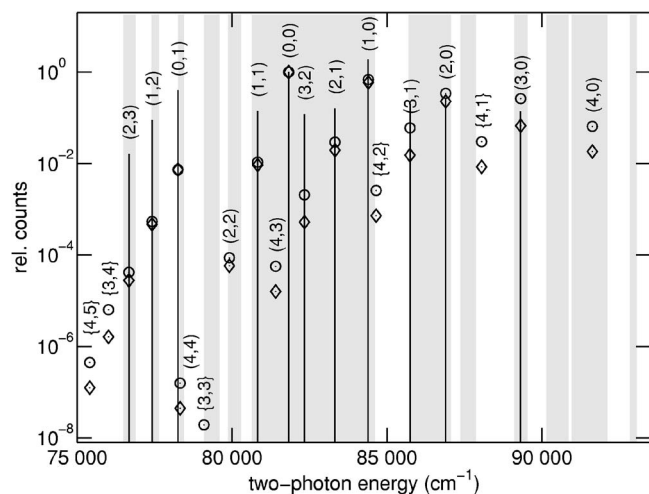


FIG. 3. Experimental (Ref. 47) and computed relative (2+1) REMPI intensities, scaled to the $(v', v'')=(0,0)$ transition. The gray areas indicate scanned regions (Ref. 47). Sticks: experimental $S_1(1)$ lines for $\text{OH}[D^2\Sigma^-(v', J') \leftarrow X^2\Pi(v'', J''=3/2)]$ transitions, \circ : efficient detection, \diamond : rapid decay model, (v', v'') : observed and calculated, $\{v', v''\}$: predicted but not scanned. The $(v', v'')=(3,2)$ transition is marked “very weak” in the accompanying paper (Ref. 13).

number of intermediate states that were used. The gray areas in Figs. 3 and 4 indicate the wavelengths where actual scans have been performed.⁴⁷ Theoretically predicted transitions which lie outside of the scanned regions are indicated with curly brackets $\{v', v''\}$. In a previous combined experimental and theoretical study, where OH/D was produced in a similar way, we estimated the vibrational temperature to be around 1700 K,⁴⁸ so the spectrum is simulated at that temperature. The spectrum was simulated under the assumption that the experimental circumstances were constant throughout the spectrum. However, this is certainly not the case due to experimental difficulties such as deterioration of the dyes during measurement, the use of different dyes, variations in OH production and its vibrational temperature, and variations in the alignment of the molecular beam with respect to

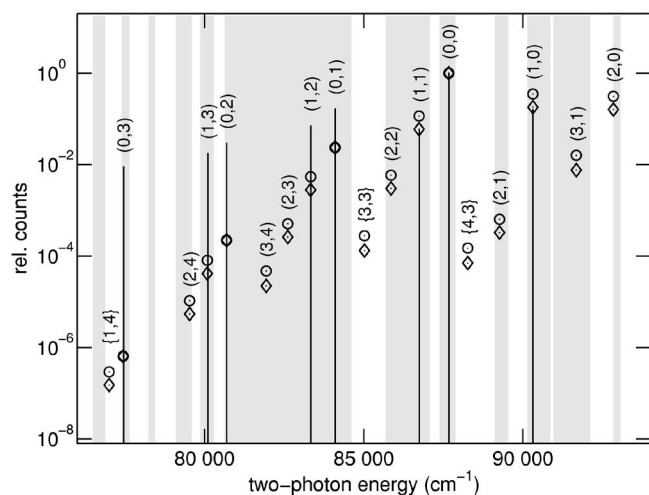


FIG. 4. As in Fig. 3, but for the $\text{OH}[3^2\Sigma^-(v', J') \leftarrow X^2\Pi(J''=3/2, v'')] S_1(1)$ transitions. The assignment of the $(v', v'')=(0,3)$ line was experimentally tentative due to an overlapping water line (Ref. 13).

TABLE III. Rotational factors S [Eq. (25)] for the $^2\Sigma^-(J') \leftarrow X^2\Pi_{3/2}(J'')$ $= |M_{J''=3/2, p''}|$ transitions.

J''	p''	$O_1(1)$	$P_1(1)$	$Q_1(1)$	$R_1(1)$	$S_1(1)$
$3/2$	e	0	$\frac{1}{150}$	0	$\frac{9}{350}$	0
$3/2$	f	0	0	$\frac{2}{75}$	0	$\frac{4}{525}$

the excitation laser.^{13,47} This means that the relative experimental line strengths are order-of-magnitude estimates at best, so we only compare the line strengths locally. That is, we compare line strengths of transitions that are close in energy since we expect the effect of variations in experimental circumstances to be less important over short energy intervals.

We see in Fig. 3 that the calculated line strengths follow the trends in the observed line strengths very well. For instance, the observed increasing line strength for the $D^2\Sigma^-(v') \leftarrow X^2\Pi(v'')$, $(v', v'')=(2,3)-(1,2)-(0,1)$ transition series is predicted by both extremes of the rate model. Also, we see that all unobserved transitions that lie in scanned regions have a lower predicted cross section than neighboring transitions that have been observed. For instance, the $(v', v'')=(4,4)$ and $(2,2)$ have much lower cross sections than the neighboring $(v', v'')=(0,1)$ and $(1,1)$ transitions. Overall, for the $D^2\Sigma^- \leftarrow X^2\Pi$ transitions both models give equally good qualitative correspondence with experimental intensities.

For the $3^2\Sigma^- \leftarrow X^2\Pi$ transitions (Fig. 4) we see similar results: both extremes predict local trends equally well, and we also find that unobserved transitions in scanned regions have much lower cross sections than observed ones.

In Table III we give the rotronic line strength factors S for the $(D/3)^2\Sigma^-(J', F_1) \leftarrow X^2\Pi_{3/2}(J''=3/2, f)$ transitions. In the experimental setup (see Paper I), a vertically polarized laser beam was put at a 90° angle with the molecular-beam axis so we have $(\phi, \theta, \chi)=(0, \pi/2, 0)$ [see Eqs. (19)–(25)]. Furthermore, molecules were aligned with $|M_{J''}|=3/2$ and

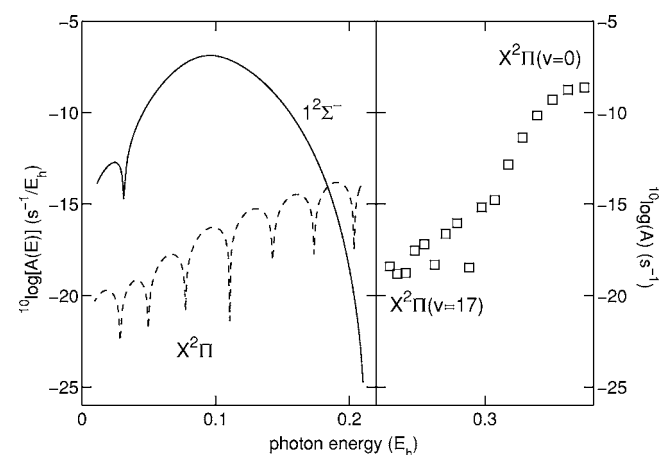


FIG. 5. Einstein A coefficients for radiation of the OH $D^2\Sigma^-(v=0)$ state to the dissociative $1^2\Sigma^-$, bound $X^2\Pi$, and dissociative $X^2\Pi$ states.

TABLE IV. Lifetimes of the $\text{OH}(D,3)^2\Sigma^-(v,J=3/2,F_1)$ states (τ) with the radiative (τ_r), the heterogeneous (gyroscopic) (τ_{he}), and the homogeneous (spin-orbit and spin-electronic) (τ_{ho}) contributions (in ns).

v	τ_r	$2^2\Pi$		$B^2\Sigma^+$	$1^4\Pi$	τ
		τ_{he}	τ_{ho}	τ_{ho}	τ_{ho}	
$D^2\Sigma^-$						
0	2.63	1.36	0.19	1.36	0.34	0.1024
1	2.88	3.00	0.39	430.01	0.18	0.1188
2	3.09	1.72	0.23	11.59	0.65	0.1537
3	3.28	4.03	0.56	6.23	3.43	0.4021
4	3.46	15.25	2.25	5.65	0.48	0.3635
$3^2\Sigma^-$						
0	2.56	0.20	0.25	0.12	0.13	0.0397
1	2.03	0.98	0.69	0.10	73.42	0.0770
2	1.71	30.15	3.63	0.10	0.37	0.0773
3	1.47	28.44	22.41	0.11	0.32	0.0839

we sum over $M_{J'}$ states. We obtain an intensity ratio for the $Q_1(1)/S_1(1)$ lines of $3\frac{1}{2}$. This is in good agreement with the experimentally observed ratios (based on the peak surface areas), which we estimated from Figs. 3 and 5 in Paper I (Ref. 13) to be between about 2 and 4.

C. Lifetimes

Figure 5 shows the Einstein A coefficients for the decay of the $D^2\Sigma^-(v=0)$ state into different continuum and discrete states. The A coefficient for decay into continuum states is in units of s^{-1}/E_h , while the unit of A for transition to discrete states is s^{-1} . Hence, we may only compare the integral over the continuum A coefficients with the bound-bound decay rates. As shown by Smith⁴⁹ and Allison and Dalgarno⁵⁰ for the case of photodissociation, the continuum A coefficient for radiative decay into the $X^2\Pi$ state connects continuously with the discrete part if it is divided by the density of vibrational states at the threshold. However, since we also wish to compare radiative decay into the continua of two different electronic states ($1^2\Sigma^-$ and $X^2\Pi$), we do not follow this procedure here.

When radiating, the Rydberg $2^2\Sigma^-$ states decay predominantly into the $1^2\Sigma^-$ state. A small contribution comes from

the lower vibrational levels of the $X^2\Pi$ ground state, while the continuum plays no important role in the decay of the $(D,3)^2\Sigma^-$ states. The patterns for the $D^2\Sigma^-$ and $3^2\Sigma^-$ states are much alike, albeit that for the $3^2\Sigma^-$ state, radiation into the $X^2\Pi$ vibrational levels is relatively less important than for the $D^2\Sigma^-$ state.

In Tables IV and V we compare lifetimes of the Rydberg $2^2\Sigma^-(J''=3/2,F_1)$ states associated with several decay processes. In order to facilitate comparison with future experiments, we report predissociation and radiative lifetimes separately, and we distinguish the lifetime associated with heterogeneous processes, $\tau_{\text{he}} = \tau_{\text{gy}}$, and that with homogeneous processes, $\tau_{\text{ho}}^{-1} = \tau_{\text{so}}^{-1} + \tau_{\text{se}}^{-1}$.

As first conjectured by van Dishoeck and Dalgarno,⁴⁵ we find that predissociation is indeed the most important line-broadening effect. The $D^2\Sigma^-$ state predissociates mainly by spin-orbit coupling with the $2^2\Pi$ and $1^4\Pi$ states. Heterogeneous processes are less important at these low rotational levels. The \hat{L}_{\pm} coupling matrix element is about $1\text{--}2\text{ cm}^{-1}$ in the bound region and thus contributes less than the spin-orbit coupling matrix elements which are about twice as large (see Table VI).

The $3^2\Sigma^-$ state also predissociates into the $2^2\Pi$ and

TABLE V. As in Table IV, but for OD.

v	τ_r	$2^2\Pi$		$B^2\Sigma^+$	$1^4\Pi$	τ
		τ_{he}	τ_{ho}	τ_{ho}	τ_{ho}	
$D^2\Sigma^-$						
0	2.59	5.84	0.23	1.37	0.51	0.1382
1	2.78	4.34	0.17	14.82	0.13	0.0710
2	2.95	9.64	0.38	2.65	55.92	0.3189
3	3.10	432.08	13.52	2.55	0.26	0.2336
4	3.24	14.12	0.53	3.37	0.43	0.2179
$3^2\Sigma^-$						
0	2.65	0.61	0.24	0.12	0.12	0.0437
1	2.21	10.18	0.92	0.08	1.73	0.0701
2	1.91	9.71	44.82	0.08	0.22	0.0583
3	1.69	2.86	4.05	0.09	0.47	0.0722

TABLE VI. Spin-orbit ($\langle f|\hat{H}_{so}|i\rangle$) and $\langle f|\hat{L}_+|i\rangle$ coupling matrix elements relevant for predissociation of the Rydberg $2^2\Sigma^-$ states. The matrix elements were computed at the crossing of the Rydberg states with the dissociative states.

$\langle f $	$\langle f \hat{H}_{so} 2^2\Sigma^- \rangle$ (cm $^{-1}$)	
	$D^2\Sigma^-$	$3^2\Sigma^-$
$2^2\Pi$	4.50	2.50
$B^2\Sigma^+$	1.10	4.60
$1^4\Pi(\Sigma=3/2)$	4.00	4.02

$\langle f $	$\langle f \hat{L}_+ 2^2\Sigma^- \rangle$ (E_h)	
	$D^2\Sigma^-$	$3^2\Sigma^-$
$2^2\Pi$	0.048 682	0.080 789

$1^4\Pi$ states, but because of a stronger spin-orbit coupling with the $B^2\Sigma^+$ state the lifetime of the $3^2\Sigma^-$ state is shorter than the lifetime of the $D^2\Sigma^-$ state.

The $2^2\Pi$, $B^2\Sigma^+$, and $1^4\Pi$ states correlate with $O(^1D)$, $O(^1S)$, and $O(^3P)$, respectively. All states correlate with the $H(^2S)$ limit. The lifetimes reported here could therefore be probed experimentally by measuring the $O(^1D, ^1S, ^3P)$ branching ratios.

There are no accurate measurements (yet) of the lifetime of the $OH[D^2\Sigma^-(v''=0)]$ state. McRaven *et al.*⁵ reported an 8-ns upper limit based on the experimental laser-pulse duration. De Beer *et al.*³ “roughly estimate” the lower lifetime limit to be $5 \times 10^{-10}[J(J+1)]^{-1}$ for the $D^2\Sigma^-(v=0, \dots, 2)$ states, which yields about 31.75 ps for the $J=3/2$ state. Here we find a lifetime of 102.4 ps, which lies in between the current experimental limits and within a factor of 3 from the estimate of de Beer *et al.*

IV. SUMMARY AND CONCLUSIONS

We computed a new set of high-quality potential-energy curves for OH/D, up to and including the Rydberg $3^2\Sigma^-$ state. Vibrational energy splittings and rotational constants for the $D^2\Sigma^-$ and $3^2\Sigma^-$ states based on these *ab initio* potentials show excellent agreement with experiment. The agreement is improved after a minor scaling of the potentials. We also report the vibrational constants G_v and rotational constants B_v for a set of unobserved levels and for the OD isotope. A new set of transition dipole moments for the doublet states of OH/D was computed and used in a calculation of the observed $(2+1)$ REMPI spectra reported in Paper I. To obtain the spectra, we include the effect of the $1^2\Sigma^-$ intermediate state by using the Seideman-Miller discrete variable representation-absorbing boundary condition method, which was originally derived for scattering and photodissociation calculations. The reason some transitions were scanned but not observed is that the two-photon cross section of these transitions is much lower than those of the observed transitions. Furthermore, relations were derived for the relative line strengths for aligned molecules at different experimental geometries and a good numerical agreement with experiment is obtained. We compute the radiative and predissociative lifetimes of the Rydberg $(D, 3)^2\Sigma^-$ states in-

cluding the effect of spin-orbit coupling and spin-electronic and gyroscopic predissociations. We find that predissociation occurs much faster than radiation, and we find the total lifetime of the $D^2\Sigma^-(v=1, J=3/2, F_1)$ state to be 102.4 ps, which lies in between currently known experimental limits.

ACKNOWLEDGMENTS

The authors thank Ad van der Avoird for carefully reading the manuscript. This research has been financially supported by the Council for Chemical Sciences of the Netherlands Organization for Scientific Research (CW-NWO).

- A. E. Douglas, *Can. J. Phys.* **52**, 318 (1974).
- I. Easson and M. Pryce, *Can. J. Phys.* **51**, 518 (1973).
- E. de Beer, M. P. Koopmans, C. A. de Lange, Y. Wang, and W. A. Chupka, *J. Chem. Phys.* **94**, 7634 (1991).
- E. de Beer, C. A. de Lange, J. A. Stephens, K. Wang, and V. McKoy, *J. Chem. Phys.* **95**, 14 (1991).
- C. McRaven, J. Alnis, B. Furneaux, and N. Shafer-Ray, *J. Phys. Chem.* **107**, 7138 (2003).
- E. F. van Dishoeck, S. R. Langhoff, and A. Dalgarno, *J. Chem. Phys.* **78**, 4552 (1983).
- J. A. Stephens and V. McKoy, *J. Chem. Phys.* **93**, 7863 (1990).
- J. A. Stephens and V. McKoy, *Phys. Rev. Lett.* **62**, 889 (1989).
- E. F. van Dishoeck and A. Dalgarno, *Icarus* **56**, 184 (1983).
- E. F. van Dishoeck and A. Dalgarno, *Icarus* **59**, 305 (1984).
- E. F. van Dishoeck, M. C. van Hemert, A. C. Alison, and A. Dalgarno, *J. Chem. Phys.* **81**, 5709 (1984).
- J. P. Morgenthaler, W. M. Harris, F. Scherb, C. M. Anderson, R. J. Oliverson, N. E. Doane, M. R. Combi, M. L. Marconi, and W. H. Smyth, *Astrophys. J.* **563**, 451 (2001).
- M. E. Greenslade, M. I. Lester, D. Č. Radenović, J. A. van Roij, and D. H. Parker, *J. Chem. Phys.* **123**, 074309 (2005), the preceding paper.
- T. Seideman and W. H. Miller, *J. Chem. Phys.* **96**, 4412 (1992).
- T. Seideman and W. H. Miller, *J. Chem. Phys.* **97**, 2499 (1992).
- T. Seideman, *J. Chem. Phys.* **98**, 1989 (1993).
- G. Herzberg, *Spectra of Diatomic Molecules*, Molecular Spectra and Molecular Structure Vol. 1 (Van Nostrand, New York, 1950).
- R. N. Zare, *Angular Momentum* (Wiley, New York, 1988).
- M. C. G. N. van Vroonhoven and G. C. Groenenboom, *J. Chem. Phys.* **116**, 1965 (2002).
- MOLPRO is a package of *ab initio* programs written by H.-J. Werner and P. J. Knowles, with contributions from R. D. Amos, A. Berning, D. L. Cooper *et al.*
- P. J. Knowles and H.-J. Werner, *Chem. Phys. Lett.* **145**, 514 (1988).
- H.-J. Werner and P. J. Knowles, *J. Chem. Phys.* **89**, 5803 (1988).
- H.-J. Werner and P. J. Knowles, *J. Chem. Phys.* **82**, 5053 (1985).
- P. J. Knowles and H.-J. Werner, *Chem. Phys. Lett.* **115**, 259 (1985).
- R. McWeeny, *Methods of Molecular Quantum Mechanics*, 2nd ed. (Academic, London, 1989), Ch. 5.
- Atomic energy levels are taken from the National Institute of Standards and Technology (NIST) atomic spectra database. See http://physics.nist.gov/cgi-bin/AtData/main_asd.
- R. A. Copeland, B. R. Chamala, and J. A. Coxon, *J. Mol. Spectrosc.* **161**, 243 (1993).
- J. R. Ackerhalt and J. H. Eberly, *Phys. Rev. A* **14**, 1705 (1976).
- M. S. Pindzola, *Phys. Rev. A* **17**, 1021 (1978).
- L. Allen, R. W. Boyd, J. Krasinski, M. S. Malcuit, and C. R. Stroud, Jr., *Phys. Rev. Lett.* **54**, 309 (1985).
- D. J. Bamford, L. E. Jusinski, and W. K. B., *Phys. Rev. A* **34**, 185 (1986).
- R. P. Saxon and J. Eichler, *Phys. Rev. A* **34**, 199 (1986).
- D. P. Craig and T. Thirunamachandran, *Molecular Quantum Electrodynamics* (Academic, London, 1984).
- R. Loudon, *The Quantum Theory of Light* (Oxford University Press, Oxford, 1973).

- ³⁵G. J. Fiechtner and J. R. Gord, *J. Quant. Spectrosc. Radiat. Transf.* **68**, 543 (2000).
- ³⁶J. D. Jackson, *Classical Electrodynamics*, 2nd ed. (Wiley, New York, 1975).
- ³⁷W. M. McLain and R. A. Harris, in *Excited States*, edited by E. C. Lin (Academic, New York, 1977), Vol. 3, pp. 1–57.
- ³⁸K. Omnidvar, *Phys. Rev. A* **22**, 1576 (1980).
- ³⁹D. T. Colbert and W. H. Miller, *J. Chem. Phys.* **96**, 1982 (1992).
- ⁴⁰G. C. Groenenboom and D. T. Colbert, *J. Chem. Phys.* **99**, 9681 (1993).
- ⁴¹H. Lefebvre-Brion and R. W. Field, *Perturbations in the Spectra of Diatomic Molecules* (Academic, New York, 1986).
- ⁴²R. Schinke, *Photodissociation Dynamics* (Cambridge University Press, Cambridge, 1993).
- ⁴³R. Colin, P.-F. Coheur, M. Kiseleva, A. C. Vandaele, and P. F. Bernath, *J. Mol. Spectrosc.* **214**, 225 (2002).
- ⁴⁴F. Mélen, J. Sauval, N. Grevesse, C. B. Farmer, C. Servais, L. Delbouille, and G. Roland, *J. Mol. Spectrosc.* **174**, 490 (1995).
- ⁴⁵E. F. van Dishoeck and A. Dalgarno, *J. Chem. Phys.* **79**, 873 (1983).
- ⁴⁶See EPAPS Document No. E-JCPSA6-123-037528 for the computed potential energy curves and dipole transition moments. This document can be reached via a direct link in the online article's HTML reference section or via the EPAPS homepage (<http://www.aip.org/pubservs/epaps.html>).
- ⁴⁷M. E. Greenslade, M. I. Lester, D. Č. Radenović, A. J. A. van Roij, and D. H. Parker (private communication).
- ⁴⁸D. Č. Radenović, A. J. A. van Roij, D. A. Chestakov, A. T. J. B. Eppink, J. J. ter Meulen, D. H. Parker, M. P. J. van der Loo, G. C. Groenenboom, M. E. Greenslade, and M. I. Lester, *J. Chem. Phys.* **119**, 9341 (2003).
- ⁴⁹A. L. Smith, *J. Chem. Phys.* **55**, 4344 (1971).
- ⁵⁰A. C. Allison and A. Dalgarno, *J. Chem. Phys.* **55**, 4342 (1971).
- ⁵¹S. R. Langhoff and E. R. Davidson, *Int. J. Quantum Chem.* **8**, 61 (1974).
- ⁵²T. H. Dunning, *J. Chem. Phys.* **90**, 1007 (1989).